Applied Physics Express 5 (2012) 102103
http://dx.doi.org/10.1143/APEX.5.102103

Reduction in Thermal Droop Using Thick Single-Quantum-Well Structure in Semipolar ($20\bar{2}\bar{1}$) Blue Light-Emitting Diodes

Chih-Chien Pan[1]*, Tao Gilbert[1], Nathan Pfaff[1], Shinichi Tanaka[1], Yuji Zhao[2], Daniel Feezell[1], James S. Speck[1], Shuji Nakamura[1,2], and Steven P. DenBaars[1,2]

[1]*Materials Department, University of California, Santa Barbara, CA 93106-5050, U.S.A.*
[2]*Electrical and Computer Engineering Department, University of California, Santa Barbara, CA 93106-9560, U.S.A.*

Received August 21, 2012; accepted September 3, 2012; published online September 26, 2012

We report on the thermal performance of the electroluminescence of 12-nm-thick single-quantum-well (SQW) InGaN blue light-emitting diodes (LEDs) grown on the semipolar ($20\bar{2}\bar{1}$) plane. At a current density 100 A/cm^2, the external quantum efficiency (EQE) decreased by 9.7% when the temperature was increased from 20 to 100 °C. Hot/cold factors were more than 0.9 at current densities greater than 20 A/cm^2. A high characteristic temperature of 900 K and low junction temperature of 68 °C were also measured using bare LED chips.

GaN-based high-power and high-efficiency light-emitting diodes (LEDs) have increasingly become a viable light source for illumination applications, such as automotive headlights, interior/exterior lighting, and full color displays. However, current commercial LEDs grown on the *c*-plane of the wurtzite crystal suffer from the quantum-confined Stark effect (QCSE) due to the large polarization-related spontaneous and piezoelectric fields.[1)] This effect causes tilted bands in the active region, resulting in the separation of electrons and holes in the active region, thus reducing the radiative recombination rate and possibly reducing the internal quantum efficiency (IQE).[2)] Moreover, IQE is further reduced with increasing drive currents and temperature, so-called efficiency droop or current droop[3–9)] and thermal droop,[10–14)] respectively. These effects limit the use of LEDs in various applications where high-current and high-temperature operation are required. Proposed mechanisms explaining current droop are mainly defect-related non-radiative recombination, Auger recombination, and carrier leakage.[3–9)] Several approaches have been used to reduce efficiency droop. For instance, large-area LED chips have been used to lower the carrier density to address the aforementioned problems by reducing the effects of Auger recombination and carrier leakage while maintaining adequate radiant flux. Reducing the carrier density by using a large-area chip comes with an associated increase in substrate cost at a time when cost reduction is a key challenge in the industry. Our group has recently demonstrated a high-efficiency small-area (chip size of ~0.1 mm^2) semipolar ($20\bar{2}\bar{1}$) blue LED with a high-quality 12-nm-thick quantum well to achieve higher than 50% external quantum efficiency (EQE) with less than 4% efficiency droop at a current density of 100 A/cm^2.[15)] For comparison, conventional *c*-plane blue LEDs[12)] have more than 40% efficiency droop at the same current density. Conventional *c*-plane blue LEDs usually suffer from significant thermal droop, and a strong decrease in light output power (LOP) and EQE with increasing temperatures.[10,11)] Thermal droop in *c*-plane LEDs can be more than 20%, as calculated using eq. (1), at 100 A/cm^2 when increasing the temperature from room temperature to 100 °C.[10,11)]

$$\text{Thermal droop (\%)} = \frac{\text{EQE(J)}_{20^\circ\text{C}} - \text{EQE(J)}_{100^\circ\text{C}}}{\text{EQE(J)}_{20^\circ\text{C}}} \times 100\% \quad (1)$$

No group has reported thermal droop of semipolar ($20\bar{2}\bar{1}$) LEDs. Here, we measured the thermal droop of semipolar LEDs for the first time showing a semipolar ($20\bar{2}\bar{1}$) 12-nm-thick single-quantum-well (SQW) blue LED with a thermal droop of only 9% at 100 A/cm^2 when the temperature is increased from 20 to 100 °C.

Semipolar ($20\bar{2}\bar{1}$) blue LEDs used in this study were grown homoepitaxially by metal organic chemical vapor deposition (MOCVD) on on-axis free-standing ($20\bar{2}\bar{1}$) GaN substrate provided by Mitsubishi Chemical. A schematic figure of the semipolar ($20\bar{2}\bar{1}$) orientation in the wurtzite crystal structure and LED structure on semipolar ($20\bar{2}\bar{1}$) free-standing GaN can be found in ref. 15. Bare LED chips from the same wafer described in ref. 15 were mounted on a ceramic plate for testing in a customized integrating sphere fitted with a thermoelectric cooler (TEC) to control the die temperature during LED testing. The output power of the LEDs was measured under pulsed current conditions with one pulse by changing the pulse width from 30 ms to 10 s depending on the magnitude of the current density to maximize radiant flux and prevent self-heating.

Figure 1 shows temperature-dependent EQE versus current density. As we can see in Fig. 1, the EQE gradually decreased with increasing temperature at different current densities probably due to the effects of non-radiative recombination, Auger recombination and carrier leakage.[3–9)] Compared with our previous work,[15)] the relatively low EQE is due to the absence of silicone encapsulation for the current experiments.

Figure 2(a) shows the EQE as a function of temperature for different current densities. As seen in Fig. 2(a), the temperature-dependent EQE curve reaches a maximum EQE at 40 A/cm^2. Figure 2(b) shows thermal droop as a function of temperature, which is calculated based on eq. (1). Thermal droops for the LED operated at 1 and 100 A/cm^2 are 22.5 and 9.7% respectively (less than 10% thermal droop when the current density is between 20 and 100 A/cm^2), when the temperature was increased from 20 to 100 °C. Reduced thermal droop was measured at 100 A/cm^2 compared with 1 A/cm^2. The difference in thermal droop between low and high current densities is explained using the recombination rate equation.[11)] At low current densities, Shockley–Read–Hall (SRH) nonradiative recombination becomes dominant over the radiative recombination. With increasing current density, the radiative recombination increases and becomes

*E-mail address: c_pan@umail.ucsb.edu

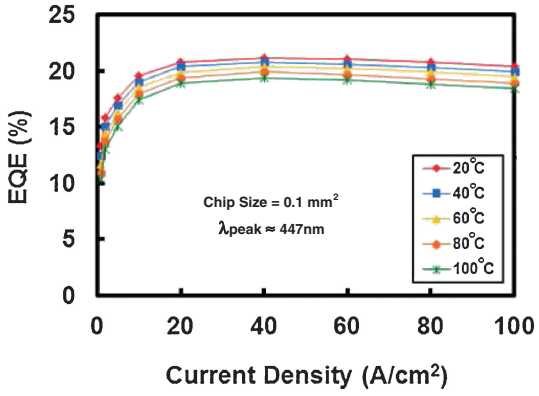

Fig. 1. External quantum efficiency versus current density under different temperatures for the semipolar (20$\bar{2}\bar{1}$) SQW blue LED.

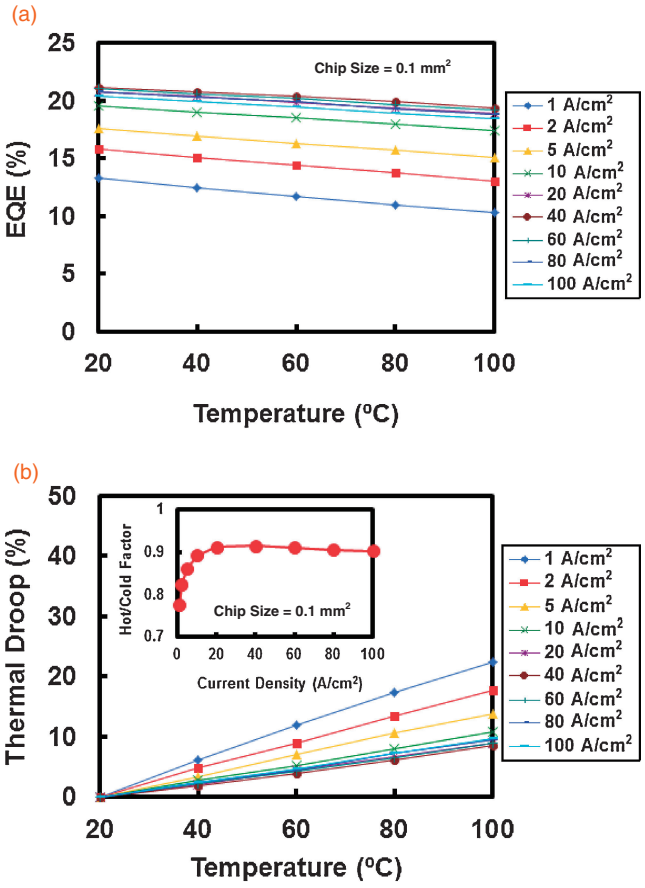

Fig. 2. Current-density-dependent (a) external quantum efficiency, and (b) thermal droop as a function of temperature for the semipolar (20$\bar{2}\bar{1}$) SQW blue LED. Inset: Hot/cold factor as a function of current density.

the dominant mechanism over SRH nonradiative recombination. Thermal droop of conventional *c*-plane LEDs was more than 20% at 100 A/cm^2 when increasing the temperature from room temperature to 100 °C.[10,11] Compared with the conventional *c*-plane blue LEDs, semipolar (20$\bar{2}\bar{1}$) blue LEDs showed a reduction in thermal droop of more than 50% over the same temperature range.

We also show hot/cold factor as a function of current density in the inset of Fig. 2(b), which is calculated based on

$$\text{hot/cold factor} = \frac{\text{EQE(J)}_{100^\circ\text{C}}}{\text{EQE(J)}_{20^\circ\text{C}}}. \quad (2)$$

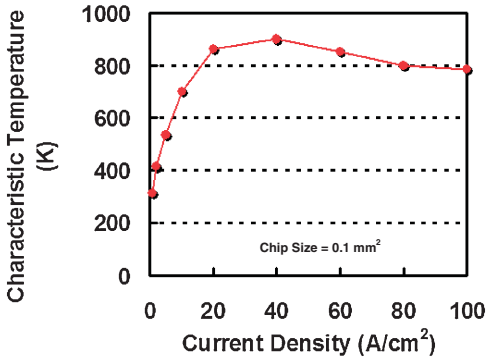

Fig. 3. Characteristic temperature (T_c) as a function of current density for the semipolar (20$\bar{2}\bar{1}$) SQW blue LED.

As we can see in the inset, the semipolar (20$\bar{2}\bar{1}$) blue LEDs can achieve hot/cold factors greater than 0.9 when the current density is greater than 20 A/cm^2. On the other hand, hot/cold factors of the conventional *c*-plane blue LEDs were calculated to be less than 0.8 under the same measurement conditions.[10,11]

As we know, the temperature dependence of the LED emission intensity is frequently described using the phenomenological equation[13]

$$I = I_{293} \exp\left(-\frac{T - 293\,\text{K}}{T_c}\right) \quad (3)$$

where I_{293} and I are the LOPs at room temperature and the operating temperature T of interest, respectively, and T_c is the characteristic temperature. Figure 3 shows T_c as a function of current density. Compared with low T_c of ~170 K for conventional *c*-plane blue LEDs in ref. 13 at a current density of 40 A/cm^2, a high T_c of nearly 900 K was achieved at the same current density for semipolar (20$\bar{2}\bar{1}$) SQW blue LEDs. A higher T_c is desirable for LEDs to improve the output power stability as a function of temperature.

We also measured the junction temperatures of semipolar (20$\bar{2}\bar{1}$) blue LEDs under different DC operating conditions. We used the forward-voltage method[16] to obtain the junction temperature of the device as

$$\frac{dV_f}{dT} = \frac{eV_f - E_g}{eT} + \frac{1}{e}\frac{dE_g}{dT} - \frac{3k}{e}. \quad (4)$$

Here, V_f is the forward voltage, e is the elementary charge, E_g is the bandgap energy, k is the Boltzmann constant, and T is the junction temperature (see ref. 16 for details).

Figure 4(a) shows DC forward voltage as a function of temperature at different current densities. In Fig. 4(a), a temperature coefficient dV_f/dT of ~−3 to −3.3 mV/K can be extracted at various current densities. DC forward voltages were measured and recorded once a thermal steady state had been reached for each current density. By using the values of dV_f/dT and corresponding DC forward voltages, we obtained the junction temperatures at each current density. As we can see in Fig. 4(b), the junction temperature is ~68 °C at 100 A/cm^2 in these semipolar (20$\bar{2}\bar{1}$) SQW blue LEDs. We also used an infrared camera to measure the chip temperature of the semipolar (20$\bar{2}\bar{1}$) SQW blue LEDs, as shown in the inset of Fig. 4(b), under a current density of 100 A/cm^2. The infrared camera showed a chip temperature of ~64 °C, which is almost the same as that obtained by the

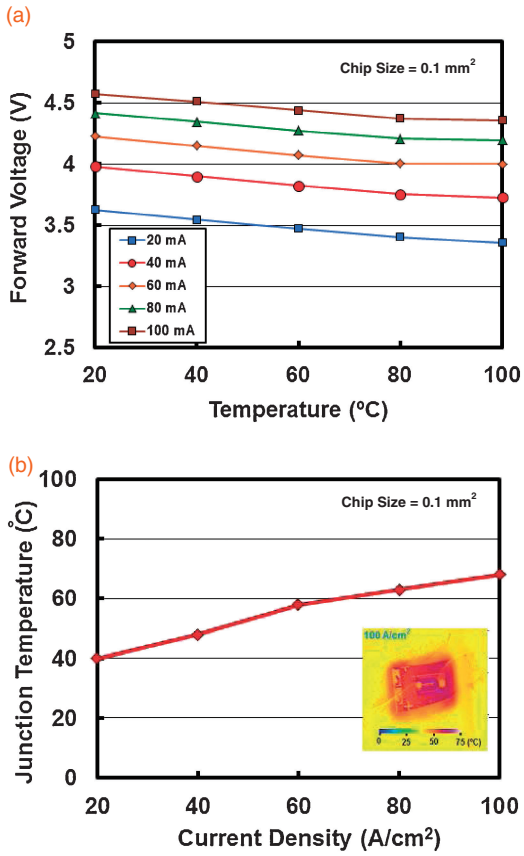

Fig. 4. (a) Forward voltage as a function of temperature, (b) junction temperature as a function of current density for the semipolar $(20\bar{2}\bar{1})$ SQW blue LED. Inset: Thermal imaging of semipolar $(20\bar{2}\bar{1})$ SQW blue LED at a current density of 100 A/cm^2.

forward-voltage method. At the DC current density up to 100 A/cm^2, the junction temperature was less than 100 °C, and the value is within the range of the temperature we used for measuring the results in Figs. 1–3.

Based on the small blue shift and narrow spectrum width in semipolar $(20\bar{2}\bar{1})$ LEDs,[15,17–19] we propose that InGaN QWs on the semipolar $(20\bar{2}\bar{1})$ plane are relatively free from indium fluctuations, resulting in a low degree of carrier localization and minimal band filling of localized states.[20,21] Ryu *et al.*[9] have recently postulated that the effective active region volume over which carriers are distributed in conventional *c*-plane InGaN QW is significantly reduced due to polarization-related electric fields, nonuniform carrier distribution, and potential fluctuations. As a result, high carrier densities are present in the active region, which exacerbate the effects of Auger recombination and carrier leakage,[3,8,22] resulting in high efficiency droop for conventional *c*-plane LEDs. In our semipolar $(20\bar{2}\bar{1})$ LEDs, polarization-related electric fields are significantly reduced; an SQW active region eliminates carrier nonuniformity issues. Additionally, the thick high-quality homogeneous InGaN layer grown at a relatively high growth temperature[18] reduces the effects of potential fluctuations and lowers the average carrier density. The result is a much larger effective active region volume than that of conventional *c*-plane LEDs. This reduces the effects of Auger recombination and carrier leakage by reducing the carrier density, resulting in a device with a low efficiency droop. When the temperature of the LED is increased, Auger recombination and carrier leakage are minimized for semipolar $(20\bar{2}\bar{1})$ LEDs due to the much lower carrier density caused by a large effective active volume as mentioned above. As a result, the thermal droop of the semipolar $(20\bar{2}\bar{1})$ LEDs is also minimized.

In summary, we demonstrated a semipolar $(20\bar{2}\bar{1})$ SQW blue LED utilizing a 12-nm-wide quantum well achieving a thermal droop of only 9.7% at 100 A/cm^2, when the temperature was increased from 20 to 100 °C. The thermal droop of the conventional *c*-plane LED was more than 20% under the same measurement conditions. Hot/cold factors of the semipolar $(20\bar{2}\bar{1})$ LEDs were more than 0.9 when the current density is greater than 20 A/cm^2. Conventional *c*-plane blue LEDs had hot/cold factors of less than 0.8 under identical measurement conditions. A high characteristic temperature T_c of 900 K was obtained for the $(20\bar{2}\bar{1})$ LED compared with 170 K of *c*-plane blue LEDs. The $(20\bar{2}\bar{1})$ semipolar blue LEDs were superior to the conventional *c*-plane LEDs in view of the efficiency droop and thermal droop.

Acknowledgments The authors would like to thank Mitsubishi Chemical Corporation for the supply of bulk GaN substrates. The authors acknowledge the Solid State Lighting and Energy Center (SSLEC) at UCSB and the support of the NSF MRSEC program (DMR 1121053) for MRL characterization facilities. A portion of this work was performed in the UCSB nanofabrication facility, part of the National Science Foundation (NSF)-funded National Nanotechnology Infrastructure Network (NNIN).

1) F. Bernardini, V. Fiorentini, and D. Vanderbilt: Phys. Rev. B **56** (1997) R10024.
2) V. Fiorentini and F. Bernardini: Phys. Rev. B **60** (1999) 8849.
3) E. Kioupakis, P. Rinke, K. T. Delaney, and C. G. Van de Walle: Appl. Phys. Lett. **98** (2011) 161107.
4) J. Hader, J. V. Moloney, and S. W. Koch: Appl. Phys. Lett. **96** (2010) 221106.
5) A. David and M. J. Grundmann: Appl. Phys. Lett. **96** (2010) 103504.
6) J. Piprek: Phys. Status Solidi A **207** (2010) 2217.
7) X. Ni, X. Li, J. Lee, S. Liu, V. Avrutin, Ü. Özgür, H. Morkoç, and A. Matulionis: J. Appl. Phys. **108** (2010) 033112.
8) M. H. Kim, M. F. Schubert, Q. Dai, J. K. Kim, E. F. Schubert, J. Piprek, and Y. Park: Appl. Phys. Lett. **91** (2007) 183507.
9) H. Y. Ryu, D. S. Shin, and J. I. Shim: Appl. Phys. Lett. **100** (2012) 131109.
10) D. S. Meyaard, Q. Shan, Q. Dai, J. Cho, E. F. Schubert, M. H. Kim, and C. Sone: Appl. Phys. Lett. **99** (2011) 041112.
11) D. S. Meyaard, Q. Shan, J. Cho, E. F. Schubert, S. H. Han, M. H. Kim, C. Sone, S. J. Oh, and J. K. Kim: Appl. Phys. Lett. **100** (2012) 081106.
12) G. Chen, M. Craven, A. Kim, A. Munkholm, S. Watanabe, M. Camras, W. Götz, and F. Steranka: Phys. Status Solidi A **205** (2008) 1086.
13) S. Chhajed, J. Cho, E. F. Schubert, J. K. Kim, D. D. Koleske, and M. H. Crawford: Phys. Status Solidi A **208** (2011) 947.
14) H. K. Lee, J. S. Yu, and Y. T. Lee: Phys. Status Solidi A **207** (2010) 1497.
15) C. C. Pan, S. Tanaka, F. Wu, Y. Zhao, J. S. Speck, S. Nakamura, S. P. DenBaars, and D. Feezell: Appl. Phys. Express **5** (2012) 062103.
16) Y. Xi, J.-Q. Xi, T. Gessmann, J. M. Shah, J. K. Kim, E. F. Schubert, A. J. Fischer, M. H. Crawford, K. H. A. Bogart, and A. A. Allerman: Appl. Phys. Lett. **86** (2005) 031907.
17) Y. Zhao, S. Tanaka, C.-C. Pan, K. Fujito, D. Feezell, J. S. Speck, S. P. DenBaars, and S. Nakamura: Appl. Phys. Express **4** (2011) 082104.
18) Y. Zhao, Q. Yan, C.-Y. Huang, S.-C. Huang, P. S. Hsu, S. Tanaka, C.-C. Pan, Y. Kawaguchi, K. Fujito, C. G. Van de Walle, J. S. Speck, S. P. DenBaars, S. Nakamura, and D. Feezell: Appl. Phys. Lett. **100** (2012) 201108.
19) C. Y. Huang, M. T. Hardy, K. Fujito, D. F. Feezell, J. S. Speck, S. P. DenBaars, and S. Nakamura: Appl. Phys. Lett. **99** (2011) 241115.
20) S. Chichibu, T. Azuhata, T. Sota, and S. Nakamura: Appl. Phys. Lett. **69** (1996) 4188.
21) Y. Narukawa, Y. Kawakami, M. Funato, S. Fujita, S. Fujita, and S. Nakamura: Appl. Phys. Lett. **70** (1997) 981.
22) Y. C. Shen, G. O. Mueller, S. Watanabe, N. F. Gardner, A. Munkholm, and M. R. Krames: Appl. Phys. Lett. **91** (2007) 141101.